

Date of publication xxxx 00, 0000, date of current version xxxx 00, 0000.

Digital Object Identifier 10.1109/ACCESS.2017.Doi Number

Phase-Based Adaptive Fractional LQR for Inverted-Pendulum-Type Robots: Formulation and Verification

Omer Saleem¹, Senior Member, IEEE, Jamshed Iqbal², Senior Member, IEEE

¹Department of Electrical Engineering, National University of Computer and Emerging Sciences (NUCES), Lahore, Pakistan.

²School of Computer Science, Faculty of Science and Engineering, University of Hull, Hull, UK

Corresponding author: Jamshed Iqbal (e-mail: j.iqbal@hull.ac.uk).

ABSTRACT The underlying principles of inverted pendulums are widely applied to develop stabilization control strategies for under-actuated robotic systems in various applications. This article methodically designs an adaptive fractional-order linear quadratic regulator to optimize the position regulation and disturbance compensation ability of an inverted-pendulum-like robot. The proposed adaptive controller is realized by employing fractional-order differentiation operators in the baseline linear-quadratic-regulator. These fractional orders are adaptively modulated via an error-phase-based online adaptation law. The AFO modulation supplements the controller's agility to efficiently steer the input trajectory as the state error's phase changes, aiding the closed-loop system in robustly rejecting the external perturbations while maintaining a time-optimal behavior. The said propositions are verified by conducting customized experimental trials on the Quanser rotary pendulum platform. The proposed adaptive controller reduces the system's transient recovery time by 35.8%, overshoots by 35.1%, control-energy expenditure by 37.2%, and offsets by 38.2% under transient disturbances, in comparison to the baseline linear quadratic regulator. The experimental data validates the superior time optimality and disturbance compensation of the proposed control law.

INDEX TERMS Adaptive control, error phase, fractional order control, LQR, rotary inverted pendulum.

I. INTRODUCTION

Rotary inverted pendulums (RIPs) are a classic control problem in robotics and control theory [1]. They serve as a benchmark platform for developing and verifying control procedures for underactuated systems that must balance an unstable object or maintain an upright position against bounded disturbances [2]. The RIP control principles are useful for designing robots that need to be kinematically stable, responsive to setpoint changes, adaptable to exogenous disturbances, and capable of performing precise motion control tasks in various environments [3]. Some common uses of RIP in robotic applications are the stabilization of self-balancing robots [4], locomotion of bipedal exoskeletons [5], and control of aerial robots [6], etc. The open-loop instability, nonlinear characteristics, and underactuated configuration of the RIP-type robots make it challenging to stabilize them under exogenous disturbances [7].

A. LITERATURE REVIEW

The scientific literature proposes numerous control procedures to address the said problem [8]. The inflexibility of the proportional-integral-derivative controllers prevents them from effectively rejecting the random disturbances [9]. Model-free neural and fuzzy controllers are typically computationally expensive owing to their reliance on large amounts of training data and qualitative rules [10, 11]. The sliding-mode controllers are highly robust against disturbances [12]. However, their inherent switching behavior disrupts the control activity, which naturally injects chattering into the state response [13]. This phenomenon eventually leads to performance degradation, mechanical wear, and actuator saturation [14]. The higher-order sliding-mode controllers (HOSMCs) can effectively reduce chattering in under-actuated systems as proposed in [15, 16]. However, they rely upon complex algorithms to compute the higher-order state

derivatives, which can be problematic in systems with limited computational abilities [16]. Moreover, the estimated higher-order state derivatives can be highly sensitive to measurement noise, and thus require auxiliary filters to avoid degraded performance [17]. Despite yielding optimal control decisions, the nominal linear quadratic regulator (LQR) lacks resilience in mitigating the effect of identification errors, parametric uncertainties, and model variations [18]. The adaptive LQR variants that employ a well-postulated self-tuning nonlinear function to dynamically adjust the state and control weighting coefficients tend to increase the flexibility of the controller design [19]. However, pre-configuring the shapes and the limits of the self-tuning functions is a laborious task [20]. The susceptibility of the model predictive controllers to noise and model mismatch reduces their ability to respond to long drifting disturbances. [21]. The model-reference adaptive controllers require a well-identified reference model to yield an optimum control effort [22].

The fractional order (FO) control combines the principles of fractional calculus with the control theory by allocating FOs to the differentiation as well as operators in the nominal control scheme [23]. The afore-stated fractional operators introduce new parameters in the control scheme, which reasonably enhances the controller's agility to effectively handle exogenous disturbances in nonlinear dynamical systems [24]. Recently, the utilization of complex-order LQR controllers has gained a lot of traction [25]. These controllers are constructed in such a manner that complex orders (COs) replace the real-numbered FOs of differentiation/integration operators of the control law [26]. Despite increasing the controller's adaptability, the CO controllers introduce a multitude of parameters that require offline tuning [27].

B. NOVEL CONTRIBUTIONS

This article formulates a novel phase-based adaptive fractional-order LQR (AFO-LQR) for an inverted-pendulum-type robot to improve the controller's time optimality and robustness against disturbances. Indeed, the traditional LQR is formulated based on the system's linearized state space model, and thus, it is not a high-performance controller on its own as it is susceptible to performance degradation under the influence of identification errors and modeling uncertainties. It is selected as the baseline controller because it is a full-state feedback controller that minimizes an energy-like quadratic performance index to yield an optimum set of compensator gains that deliver optimal control decisions while preserving the system's asymptotic convergence as long as the necessary stability conditions are met (discussed in Section II(B)). To enhance the disturbance rejection capacity of this optimal and stable controller, the differential operators of LQR are replaced with self-adjusting FO operators in this work. The said FOs are dynamically adjusted via a pre-calibrated phase-based modulator to avoid performance limitations and compromises imposed by fixed FOs. This augmentation supplements the LQR's self-learning capability, which

increases its adaptability to flexibly manipulate the damping control activity as the operating conditions change. The key contributions of this article are listed below:

- Constitution of the adaptive FO-LQR law.
- Formulation of a phase-based modulator to online adapt the controller's FOs using pre-configured hyperbolic tangent functions (HTFs).
- Verification of the adaptive FO-LQR law by conducting hardware experiments on the Quanser RIP setup [1].

The phase-based modulator autonomously modulates the FOs of the FO-LQR between -1 and $+1$ in response to the system's state-error-phase, which dynamically re-structures the control law to predominantly exhibit derivative action as the response deviates from the setpoint and integral action as it converges. Consequently, the system delivers rapid reference tracking concurrent with robust dampening against large transients while reducing the control requirements. The employment of HTF ensures a smooth transition of the FOs and, hence, the control structure as the error phase changes.

An online adaptive controller that undertakes to self-adjust the FOs between -1 and $+1$ to mutate the FO-LQR for RIP-type robots from a derivative-type to an integral-type control law, as the error phase changes, has not yet been implemented in the academic literature. Hence, the article attempts to realize the prescribed novel concept.

C. RELATIVE BENEFITS

The proposed control law addresses the gaps and limitations associated with the state-of-the-art controllers discussed in Section I(A). Unlike the model-free linear controllers discussed above, the proposed scheme exhibits an asymptotically stable control behavior. The proposed arrangement synergistically combines the beneficial features of the integral and derivative control operators in the PID controllers by smoothly sliding between the integral and derivative control regions as the error phase conditions vary. This smooth commutation also prevents high chattering induced by the hard limits imposed by the conventional SMC reaching law. The optimal controller gains are delivered by the LQ optimization, where the FOs are adapted online between -1 and $+1$ using HTFs. Unlike HOSMCs, the FO of the derivative operator does not exceed $+1$. Hence, the estimation of higher-order derivatives is avoided, which grants the controller immunity against sensor noise. Similarly, the FO of the derivative operator does not go below -1 , which prevents the controller from actuator saturation caused by the integral wind-up. The FOs can be easily estimated using the computational resources available. Unlike the model-free neuro-fuzzy controllers, the proposed adaptation scheme does not require large sets of fuzzy rules or training data. They can be simply realized using algebraic equations that can be solved in a single step. This prevents putting excessive computation burden on the embedded processor.

The proposed AFO-LQR scheme also improves considerably upon the conventional fixed FO-LQR law as well as the CO-

PID control law used for RIP systems proposed in [25]. Firstly, the FO- or CO-PID controllers increase the LQ controller's design flexibility, however, the accurate selection of an optimal set of FOs is a very laborious task. The proposed scheme uses HTFs to obviate the necessity to tune the fixed fractional or complex orders offline. Secondly, fixed fractional (or complex) orders cannot adjust to changing conditions or dynamics within the system. This lack of flexibility can lead to suboptimal performance in environments where errors vary rapidly over time. Consequently, the systems may exhibit higher overshoots and longer settling times compared to adaptive counterparts that can continuously tune their parameters. This eventually leads to potential control energy wastage and increased control costs. The proposed controllers equipped with adaptive FOs address all the aforementioned problems, by demonstrating enhanced robustness and better handling of disturbances and uncertainties.

The remainder of the article is structured as described here: the RIP's dynamics and the nominal LQR linked with it are discussed in Section II. The AFO-LQR is constituted in Section III. The outcomes of experimental trials are examined in Section IV. Section V presents the formal conclusion.

II. SYSTEM DESCRIPTION

The RIP is a pendulum mounted on a rotating base containing a DC servo motor-driven rotary joint that supports a horizontal arm, as shown in Fig. 1 [1]. The energy controller actuates the motor to rotate the arm. This rotation swings up the unactuated vertical pendulum rod until it inverts itself. Once inverted, the state feedback controller continues to balance the rod vertically by dynamically re-adjusting the motor's control input. The instantaneous positions of the rod and arm are referred to as θ and α , respectively. The positions and velocities of each link are measured via two encoders, which are installed with the pendulum's pivot and the shaft of the motor, respectively.

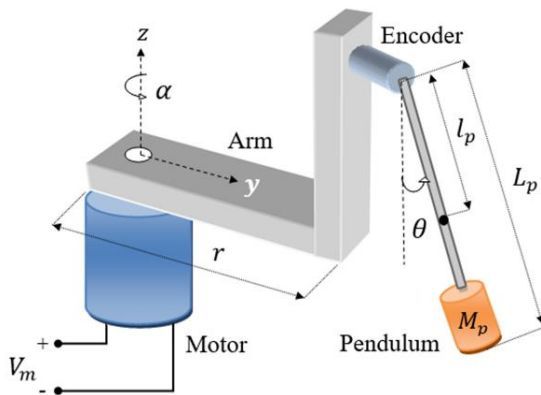


FIGURE 1. Simplified diagram of an RIP platform [1].

A. MATHEMATICAL MODELING

The RIP's linear equations of motion are derived via the Euler-Lagrange technique, as shown below [28].

$$\ddot{\theta} = \frac{1}{W} \left(M_p l_p g (J_e + M_p r^2) \theta - \frac{r M_p l_p K_t K_m}{R_m} \dot{\alpha} + \frac{r M_p l_p K_t}{R_m} V_m \right) \quad (5)$$

$$\ddot{\alpha} = \frac{1}{W} \left(r M_p^2 l_p^2 g \theta - \frac{(J_p + M_p l_p^2) K_t K_m}{R_m} \dot{\alpha} + \frac{(J_p + M_p l_p^2) K_t}{R_m} V_m \right) \quad (6)$$

$$\text{such that, } W = J_e J_p + M_p r^2 J_p + M_p l_p^2 J_e$$

Table I describes the modeling parameters indicated in (1) and (2), [19]. In state space, a linear system is described as,

$$\dot{x}(t) = \mathbf{A}x(t) + \mathbf{B}u(t), \quad y(t) = \mathbf{C}x(t) + \mathbf{D}u(t) \quad (7)$$

where, \mathbf{A} is the system matrix, \mathbf{B} is the input matrix, \mathbf{C} is the output matrix, \mathbf{D} is the feed-forward matrix, and $y(t)$ is the output vector. The system's model is presented in the block diagram in Fig. 2. The control input as well as the state vector of the RIP system are provided in (8), [7, 29].

$$u(t) = V_m(t), \quad x(t) = [\alpha(t) \quad \theta(t) \quad \dot{\alpha}(t) \quad \dot{\theta}(t)]^T \quad (8)$$

The state space matrices of the RIP are given by (9), [29].

$$\mathbf{A} = \begin{bmatrix} 0 & 0 & 1 & 0 \\ 0 & 0 & 0 & 1 \\ 0 & a_1 & a_2 & 0 \\ 0 & a_3 & a_4 & 0 \end{bmatrix}, \quad \mathbf{B} = \begin{bmatrix} 0 \\ 0 \\ b_1 \\ b_2 \end{bmatrix}, \quad \mathbf{C} = \begin{bmatrix} 1 & 0 & 0 & 0 \\ 0 & 1 & 0 & 0 \\ 0 & 0 & 1 & 0 \\ 0 & 0 & 0 & 1 \end{bmatrix}, \quad \mathbf{D} = \begin{bmatrix} 0 \\ 0 \\ 0 \\ 0 \end{bmatrix} \quad (9)$$

where,

$$a_1 = \frac{r M_p^2 l_p^2 g}{W}, \quad a_2 = \frac{-K_t K_m (J_p + M_p l_p^2)}{W R_m},$$

$$a_3 = \frac{M_p l_p g (J_e + M_p r^2)}{W}, \quad a_4 = \frac{-r M_p l_p K_t K_m}{W R_m},$$

$$b_1 = \frac{K_t (J_p + M_p l_p^2)}{W R_m}, \quad b_2 = \frac{r M_p l_p K_t}{W R_m}.$$

TABLE I
MODEL SPECIFICATIONS OF THE QUANSER RIP [19]

Symbol	Parameter details	Value	Unit
R_m	DC motor's resistance	3.30	Ω
L_m	DC motor's inductance	47.0	mH
K_t	DC motor's torque constant	0.028	Nm/A
K_m	Motor's back EMF constant	0.028	Vs/rad
J_e	Shaft's moment-of-inertia	0.000123	kgm ²
r	Rotational arm's length	0.083	m
M_{arm}	Rotational arm's mass	0.028	kg
M_p	Pendulum's mass	0.027	kg
l_p	Pendulum's center-of-mass	0.153	m
L_p	Pendulum's length	0.191	m
J_p	Pendulum's moment-of-inertia	0.00011	kgm ²
g	Acceleration due to Gravity	9.810	m/s ²

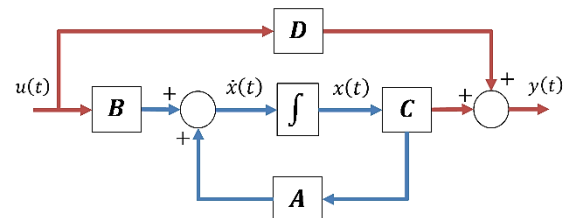


FIGURE 2. Block diagram representation of the state space model.

B. LQR FORMULATION

The LQR uses the state space model and full state feedback of a linear dynamic system to stabilize and control its behavior [1, 18]. The quadratic cost function of states and input, given by (10), is minimized by using the Hamilton-Jacobi-Bellman equation [30].

$$J_{lq} = \frac{1}{2} \int_0^{\infty} [x(t)^T \mathbf{M}x(t) + u(t)^T \mathbf{S}u(t)] dt \quad (10)$$

where, $\mathbf{M} \in \mathbb{R}^{4 \times 4}$ is the positive semidefinite state cost matrix, and $\mathbf{S} \in \mathbb{R}$ is the positive-definite control input cost matrix. For the given RIP system, the \mathbf{M} and \mathbf{S} matrices are symbolically denoted as follows.

$$\mathbf{S} = \rho, \quad \mathbf{M} = \text{diag}(q_\alpha \quad q_\theta \quad q_{\dot{\alpha}} \quad q_{\dot{\theta}}) \quad (11)$$

The parametrization of the \mathbf{M} and \mathbf{S} matrices is discussed in the following subsection. The linear optimal control law acquired by minimizing the cost function is expressed in (12).

$$u(t) = -\mathbf{K}x(t) \quad (12)$$

where, $\mathbf{K} = [k_\alpha \quad k_\theta \quad k_{\dot{\alpha}} \quad k_{\dot{\theta}}]$ is the state compensator gain vector. The LQR law can also be written as shown below.

$$u(t) = -k_\alpha \dot{\alpha}(t) - k_\theta \theta(t) - k_{\dot{\alpha}} \dot{\alpha}(t) - k_{\dot{\theta}} \dot{\theta}(t) \quad (13)$$

The gain vector is calculated as shown in (14).

$$\mathbf{K} = \mathbf{S}^{-1} \mathbf{B}^T \mathbf{P} \quad (14)$$

where \mathbf{P} is a positive-definite symmetric matrix, which is obtained by solving the continuous-time Algebraic Riccati Equation given by (15).

$$\mathbf{A}^T \mathbf{P} + \mathbf{P} \mathbf{A} - \mathbf{P} \mathbf{B} \mathbf{S}^{-1} \mathbf{B}^T \mathbf{P} + \mathbf{M} = 0 \quad (15)$$

Stability proof: The Lyapunov-stability of the LQR is proven via the function expressed in (16).

$$Z(t) = x(t)^T \mathbf{P}(t)x(t) > 0, \quad \text{where } x(t) \neq 0 \quad (16)$$

The first derivative of $Z(t)$ is derived as follows [7].

$$\dot{Z}(t) = 2(x(t)^T \mathbf{P} \dot{x}(t)) \quad (17)$$

$$= x(t)^T (\mathbf{A}^T \mathbf{P} + \mathbf{P} \mathbf{A})x(t) - 2x(t)^T (\mathbf{P} \mathbf{B} \mathbf{S}^{-1} \mathbf{B}^T \mathbf{P})x(t)$$

The expression $\dot{Z}(t)$ is simplified by inserting equation (15) in (17), as shown below.

$$\dot{Z}(t) = -x(t)^T \mathbf{M}x(t) - x(t)^T (\mathbf{P} \mathbf{B} \mathbf{S}^{-1} \mathbf{B}^T \mathbf{P})x(t) \quad (18)$$

The derivative $\dot{Z}(t) < 0$ as long as $\mathbf{M} = \mathbf{M}^T \geq 0$ and $\mathbf{S} = \mathbf{S}^T > 0$, which guarantees the LQR's asymptotic stability.

C. CONTROLLER PARAMETERIZATION

The cost function indicated in (19) is minimized in order to effectively optimize the controller parameters offline.

$$J_e = \int_0^T [(e_\alpha(t))^2 + (e_\theta(t))^2 + (u(t))^2] dt \quad (19)$$

where, $e_\alpha(t) = \alpha(t) - \alpha(0)$ and $e_\theta(t) = \theta(t) - \pi$ represent the error in the arm's position and rod's position, relative to the reference, respectively. The rod's reference positions is π rad., and the arm's reference is its initial position, $\alpha(0)$. The state and control costs are selected between 0 and 100 [1]. An illustration of the procedure used to tune the parameters is provided in Fig. 3 [1]. Section IV discusses the procedure used to conduct the experimental trials for parameter tuning. The tuning is initiated with $\mathbf{S} = 1$ and $\mathbf{M} = \text{diag}(1 \quad 1 \quad 1 \quad 1)$.

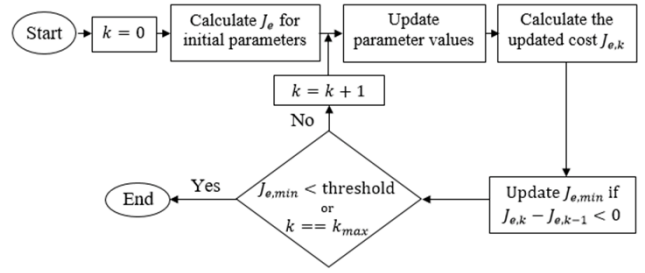


FIGURE 3. Parameter selection process [1].

Every trial involves updating the parameters suitably, manually erecting the pendulum rod, and balancing it for a period of 10.0 sec. to calculate the cost of the present trial $J_{e,k}$; where, k is the trial number. The tuning process searches the parameter range while tracking the cost function's descending gradient [31]. The local minimum-cost $J_{e,min}$ is updated if the current cost ($J_{e,k}$) is less than the cost of the prior trial ($J_{e,k-1}$). Once the maximum number of trials (k_{max}) are completed or the $J_{e,min}$ attains a pre-determined threshold value, the exploration for the optimum solutions is concluded.

The said threshold is determined based on empirical testing via pilot algorithmic runs. By conducting preliminary runs of the tuning algorithm with various thresholds and evaluating the resulting parameters, the aforementioned thresholds are selected that balance computational resource utilization and solution quality while avoiding premature termination of the tuning algorithm. In this research, the $J_{e,min}$ for initial settings of \mathbf{S} and \mathbf{M} is recorded as $J_{e,min}^0 \approx 0.89 \times 10^6$. A scaled-down value of $J_{e,min}^0$ is then used as the stopping criteria. A scale of 0.01 is empirically selected to avoid unnecessary computational burden and ensure quicker convergence of the algorithm. A larger scale value puts an excessive recursive computational burden while a smaller one leads to premature termination. Thus, the algorithm is terminated when $J_{e,min}$ approaches $0.01 J_{e,min}^0$. Correspondingly, the values of the threshold for $J_{e,min}$ and k_{max} are preset at 1×10^4 and 30, respectively [1].

The optimized set of control and state costs are $\mathbf{S} = 1.02$ and $\mathbf{M} = \text{diag}(32.8 \quad 52.2 \quad 6.1 \quad 2.5)$, respectively. The state compensator gains thus computed using (13) are $\mathbf{K} = [-6.21 \quad 130.56 \quad -4.22 \quad 17.83]$.

III. PROPOSED CONTROL PROCEDURE

This section systematically formulates the proposed phase-based adaptive FO-LQR law for the RIP system.

A. FRACTIONAL-ORDER LQR

Fractional calculus generalizes the traditional calculus operators of differentiation and integration to non-integer orders or fractional orders [32]. It provides a more nuanced understanding of systems with complex dynamics. The incorporation of fractional-order elements into the control system aids in addressing various challenges to achieve improved performance in complex dynamical systems [33].

The symbol D^λ represents the fractional mathematical operator; where, λ is the operator's FO. The definitions of FO operators, given by Gruunwald-Letnikov, Riemann-Liouville, and Caputo, are expressed as follows [32].

$$D^\lambda f(t) = \lim_{h \rightarrow 0} \frac{1}{h^\lambda} \sum_{i=0}^{(t-a)/h} (-1)^i \binom{\lambda}{i} f(t - ih) \quad (21)$$

where, $\binom{\lambda}{i} = \Gamma(\lambda + 1) / \Gamma(i + 1) \Gamma(\lambda - i + 1)$, and h is the step size.

$$D^\lambda f(t) = \frac{1}{\Gamma(n - \lambda)} \frac{d^n}{dt^n} \int_a^t \frac{f(\tau)}{(t - \tau)^{\lambda - n + 1}} d\tau \quad (20)$$

where, $\Gamma(x)$ is the Euler gamma function, n is an integer such that $n - 1 < \lambda < n$.

$$D^\lambda f(t) = \frac{1}{\Gamma(\lambda - n)} \int_a^t \frac{f^n(\tau)}{(t - \tau)^{\lambda - n + 1}} d\tau \quad (22)$$

In FO control systems, the control law includes fractional-order integrators and differentiators instead of their traditional integer-order counterparts [23]. This approach increases the flexibility in controller design, which enables it to exhibit behaviors that are not achievable with integer-order controllers. Thus, the fractional calculus is combined with the nominal LQR to realize the FO-LQR law [24]. The FO-LQR law is expressed in (23).

$$u(t) = -k_\alpha \alpha(t) - k_\theta \theta(t) - k_\alpha (D^\beta \alpha(t)) - k_\theta (D^\gamma \theta(t)) \quad (23)$$

Apart from the original state-compensator gains, the fractional calculus introduces two additional parameters in the modified control scheme in the form of the FOs of the differential operators, β and γ . The inclusion of these parameters further enhances the controller's agility. The FO-LQR law can also be written as given by (24).

$$u(t) = u_\alpha(t) + u_\theta(t) \quad (24)$$

where, $u_\alpha(t) = -k_\alpha \alpha(t) - k_\alpha (D^\beta \alpha(t))$

and, $u_\theta(t) = -k_\theta \theta(t) - k_\theta (D^\gamma \theta(t))$

The schematic of the AFO-LQR structure is illustrated in Fig. 4. The transfer functions of $u_\alpha(t)$ and $u_\theta(t)$ are given below.

$$\frac{U_\alpha(s)}{\alpha(s)} = -k_\alpha - k_\alpha s^\beta, \quad \frac{U_\theta(s)}{\theta(s)} = -k_\theta - k_\theta s^\gamma \quad (25)$$

The fractional elements s^β and s^γ are difficult to implement due to their non-integer nature. The Oustaloup filter is thus used to approximate these fractional elements [25].

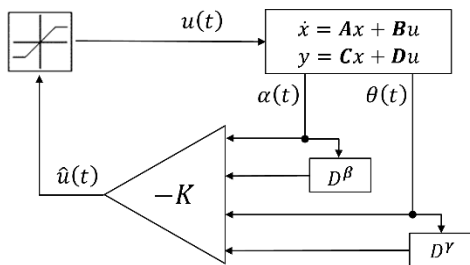


FIGURE 4. Schema of the FO-LQR scheme.

The approximation of the fractional element s^λ via the Oustaloup filter is presented in (26).

$$s^\lambda = V \prod_{i=1}^N \frac{1 + (s/w_{z,i})}{1 + (s/w_{p,i})} \quad (26)$$

$$\text{such that, } w_{z,i} = w_l (w_h/w_l)^{2i-1-\lambda/2N}, \\ w_{p,i} = w_l (w_h/w_l)^{2i-1+\lambda/2N}$$

where, N is the filter's order, w_h is the upper cut-off frequency, and w_l is the lower cut-off frequency of the filter. The V is evaluated such that $(j\omega)^\lambda = 1$ at 1.0 rad/s. The specifications of the said filter utilized in this work are $N = 5$, $w_l = 10^{-2}$ rad/s, and $w_h = 10^2$ rad/s [25].

The LQR's asymptotic stability is guaranteed as long as $\mathbf{M} = \mathbf{M}^T \geq 0$ and $\mathbf{S} = \mathbf{S}^T > 0$. These stability conditions are also sufficient for FO-LQR because the proposed scheme is not targeting the state compensator gains, instead the estimates of the state derivatives being fed to the LQR are being modified by the FO operation, as shown in Fig. 4.

To realize the fixed FO-LQR law, the parameters β and γ are optimized offline using the procedure prescribed in Section II (C). The values of β and γ are chosen from the range $[-1, 1]$. The FOs thus selected are $\beta = 0.755$ and $\gamma = 0.782$. However, the fixed setting of FOs does not always yield a robust-optimal control effort as they lack the necessary degrees of freedom to address the abrupt variations system's phase [33]. This problem can be potentially addressed by adaptively modulating the FOs, β and γ , as discussed below.

B. PROPOSED ADAPTIVE FRACTIONAL-ORDER LQR

The FOs linked with the FO-LQR law are dynamically adjusted in response to changes in the system's state error phase, which flexibly reshapes the control trajectory [34]. The knowledge of the state error phase enables the control law to realize whether the system's states (α and θ) are deviating from or returning to the setpoint [35]. The knowledge of the error phase is used in conjunction with the following set of rules to constitute the FO adaptation mechanism [36].

1. When the states deviate from the reference, the FOs are varied between 0 and 1 to enhance the proportional-derivative (PD) driven control action, which improves the transient response speed, dampens the overshoots, and efficiently reverts their direction of motion.
2. When the states are returning to the reference, the FOs are varied between -1 and 0 to strengthen the proportional-integral (PI) driven control action, which improves the system's tracking by accelerating the state's convergence to the reference while attenuating the steady-state oscillations.

These rules increase the system's adaptability to reject disturbances [35]. They are mathematically realized via a smooth and odd-symmetric nonlinear function that is bounded between -1 and $+1$. Hence, the HTF is used to implement the FO adaptation law because its waveform complies with the

aforementioned properties [36]. The general expression used to online adapt an FO is presented in (27).

$$\lambda(t) = \tanh(\delta_x g_x(t)) \quad (27)$$

where $\lambda(t)$ is an arbitrary time-varying FO, $\tanh(\cdot)$ represents the HTF, δ_x is the HTF's variation rate. Since the waveform of the HTF is restricted between -1 and $+1$, the variations in the FOs are also confined within this range. The variable $g_x(t)$ is a phase detector of the following form [26].

$$g_x(t) = (e_x(t))^3 \text{sign}(\dot{e}_x(t)) \quad (28)$$

where $\text{sign}(\cdot)$ is a signum function as shown below.

$$\text{sign}(\dot{e}_x(t)) = \begin{cases} +1, & \text{if } \dot{e}_x(t) > 0 \\ 0, & \text{if } \dot{e}_x(t) = 0 \\ -1, & \text{if } \dot{e}_x(t) < 0 \end{cases} \quad (29)$$

The waveform of $\lambda(t)$ is shown in Fig. 5 [36]. The variable $g_x(t)$ notifies the FO-LQR regarding the error phase [36]. An arbitrary under-damped system's error profile, shown in Fig. 6, can be chopped into four distinct phases; namely, A, B, C, and D. The variables e_x and \dot{e}_x have the same polarities in phases A and C, which suggests that states are deviating from the reference. Hence, $g_x(t)$ becomes positive and contributes to a PD-driven control effort. Contrarily, the e_x and \dot{e}_x variable have opposite polarities in phases B and D, which suggests that the states are returning towards the reference. Hence, $g_x(t)$ becomes negative and contributes to a PI-driven control effort. The inclusion of $g_x(t)$ in $\lambda(t)$ guarantees enhanced response speed with strong damping against disturbances. A map correlating the FO variations in response to phase changes is shown in Table II.

The error-cube signal $(e_x(t))^3$ in $g_x(t)$ creates distinctive amplified and suppressed error zones (as shown in Fig. 3), which renders a sharp increase in the FO's magnitude under large error conditions, and vice versa [37].

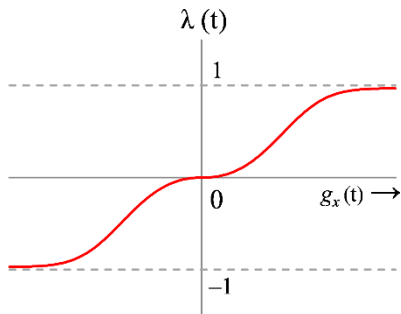


FIGURE 5. Waveform of the FO adaptation function [36].

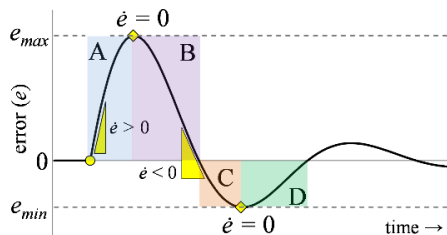


FIGURE 6. Error variation in an arbitrary under-damped system [36].

TABLE II
FO VARIATION IN RESPONSE TO PHASE CHANGES

Phase	e_x	\dot{e}_x	g_x	Response	Action	FO variation
A	> 0	> 0	> 0	Deviating	PD-type	$0 \leq \beta \leq 1,$ $0 \leq \gamma \leq 1$
B	> 0	< 0	< 0	Converging	PI-type	$-1 \leq \beta \leq 0,$ $-1 \leq \gamma \leq 0$
C	< 0	< 0	> 0	Deviating	PD-type	$0 \leq \beta \leq 1,$ $0 \leq \gamma \leq 1$
D	< 0	> 0	< 0	Converging	PI-type	$-1 \leq \beta \leq 0,$ $-1 \leq \gamma \leq 0$

The cube operation also serves to maintain the odd symmetry of the error variable. The formulae thus designed to adaptively modify $\beta(t)$ and $\gamma(t)$ are presented in (30).

$$\beta(t) = \tanh(\delta_\alpha g_\alpha(t)), \quad \gamma(t) = \tanh(\delta_\theta g_\theta(t)) \quad (30)$$

where, $g_\alpha(t) = (e_\alpha(t))^3 \text{sign}(\dot{e}_\alpha(t))$,

and, $g_\theta(t) = (e_\theta(t))^3 \text{sign}(\dot{e}_\theta(t))$

The variances δ_α and δ_θ are determined from the span $[0, 1]$ by using the afore-described optimization scheme. The variances thus chosen are $\delta_\alpha = 0.082$ and $\delta_\theta = 0.215$. The proposed adaptive FO-LQR (or AFO-LQR) law is expressed in (31).

$$\hat{u}(t) = -k_\alpha \alpha(t) - k_\theta \theta(t) - k_\alpha (D^{\beta(t)} \alpha(t)) - k_\theta (D^{\gamma(t)} \theta(t)) \quad (31)$$

The smooth commutation of the FOs between -1 and $+1$ aids in autonomously mutating the control law from a PD-type to a PI-type controller as the error phase changes. The schematic of the AFO-LQR structure is illustrated in Fig. 5.

IV. EXPERIMENTAL ANALYSIS

The experimental cases employed to benchmark the AFO-LQR's behavior with nominal LQR are discussed below.

A. HARDWARE PLATFORM

The controllers are investigated by conducting customized experiments on the Quanser RIP depicted in Fig. 8. The NI-ELVIS DAQ board records the encoder measurements of α and θ at a sampling frequency of 1000 Hz. The control application receives this data serially at a baud rate of 9600 bps.

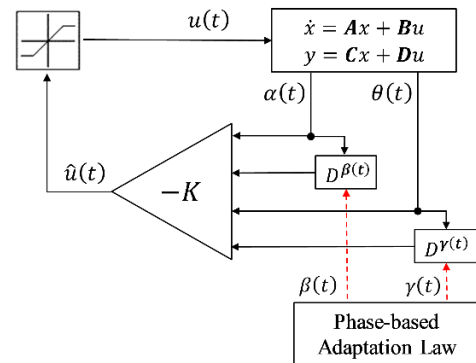


FIGURE 7. Schema of the proposed AFO-LQR scheme.

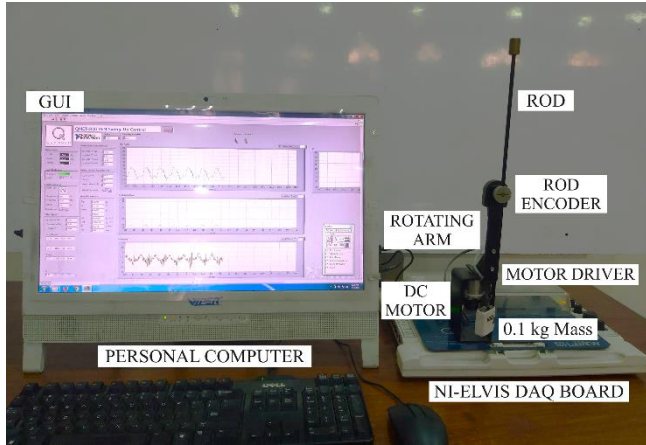


FIGURE 8. Quanser rotary inverted pendulum setup.

The LabVIEW software, operating on a 64-bit, 1.70 GHz Intel® personal computer with 12.0 GB RAM, is used to implement the customized control application. The control application also comprises a customized graphical user interface that illustrates the state and control variations. To prevent the DC motor from overheating and saturation, the control scheme uses a saturation function to confine the consequent voltage control commands within ± 18.0 V (See Fig. 7). The onboard motor driver circuit receives the modulated control signals serially to actuate the motor appropriately, and thus, self-balance the RIP.

B. EXPERIMENTAL CASES AND OUTCOMES

The following experiments are carried out to determine each controller's effectiveness. Every experiment involves setting up the rod and letting it self-balance vertically.

1. *Reference tracking*: In this experiment, the ability of the arm and rod to track their respective reference positions in the absence of disturbances is evaluated. The profiles of $\alpha(t)$, $\theta(t)$, $V_m(t)$, $\beta(t)$ and $\gamma(t)$ are depicted in Fig. 9.
2. *Impulse disruptions*: In this experiment, a pulse signal with a peak voltage of -5.0 V and a duration of 100 msec. is injected in $V_m(t)$ at discrete intervals to test the controller's resistance to impulsive forces. To conduct this experiment, the "pulse pattern" block is chosen from the function's palette in Labview's block diagram tool [38]. The input parameters of the pulse generator are appropriately configured to attain the desired pulse width and amplitude. When activated, the said generator injects a pulse directly into the system's control input signal. The profiles of $\alpha(t)$, $\theta(t)$, $V_m(t)$, $\beta(t)$ and $\gamma(t)$ are shown in Fig. 10.
3. *Step disruption*: In this experiment, a step signal of -5.0 V is injected in $V_m(t)$ at $t \approx 6.0$ sec to test the controller's resilience to load changes. The profiles of $\alpha(t)$, $\theta(t)$, $V_m(t)$, $\beta(t)$ and $\gamma(t)$ are shown in Fig. 11.

4. *Sinusoidal disruption*: In this experiment, a sinusoidal signal $d(t) = \sin(20\pi t)$, is introduced in $V_m(t)$ to examine the controller's robustness against sensor and mechanical noise. The profiles of $\alpha(t)$, $\theta(t)$, $V_m(t)$, $\beta(t)$ and $\gamma(t)$ are shown in Fig. 12.

5. *Model uncertainties*: In this experiment, a 0.1 kg mass is manually attached with the hook underneath the pendulum's rod-arm assembly at $t \approx 6.0$ sec, as shown in Fig. 13, to evaluate the controller's adaptability against the state fluctuations caused by the model variations. This arrangement creates a loading effect on the motor and changes the mass of the pendulum-arm assembly, which sets up the desired model uncertainty. The consequent modification incurred in the coefficients of the matrices A and B leads to a sudden variation in the system's actual model, creating a difference between the actual and simulated models of the system. The profiles of $\alpha(t)$, $\theta(t)$, $V_m(t)$, $\beta(t)$ and $\gamma(t)$ are shown in Fig. 14.

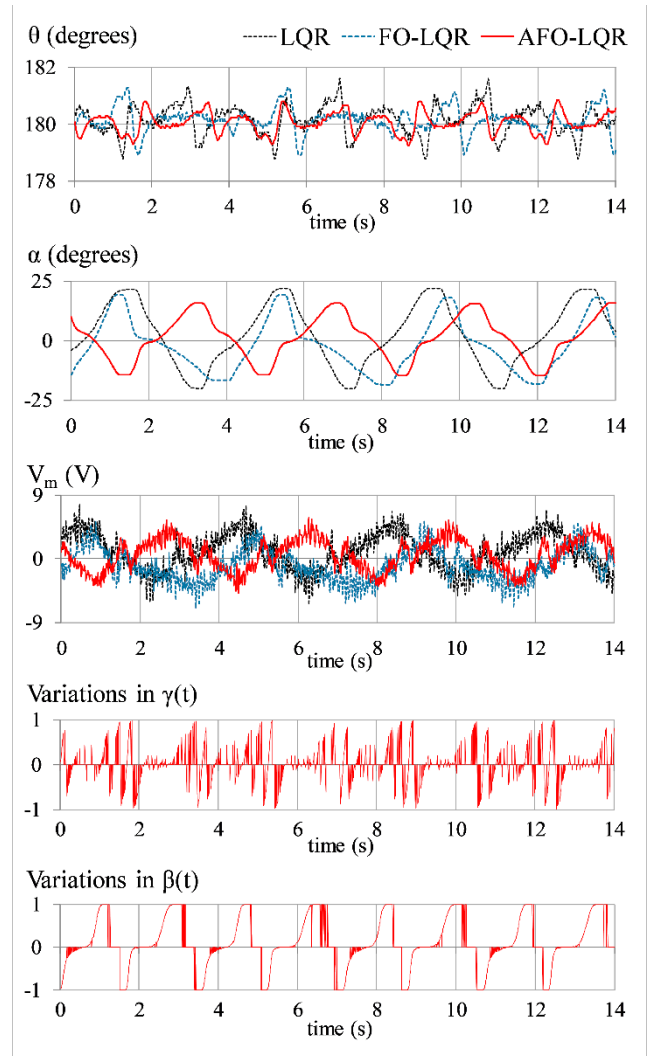


FIGURE 9. System's position regulation in disturbance-free conditions.

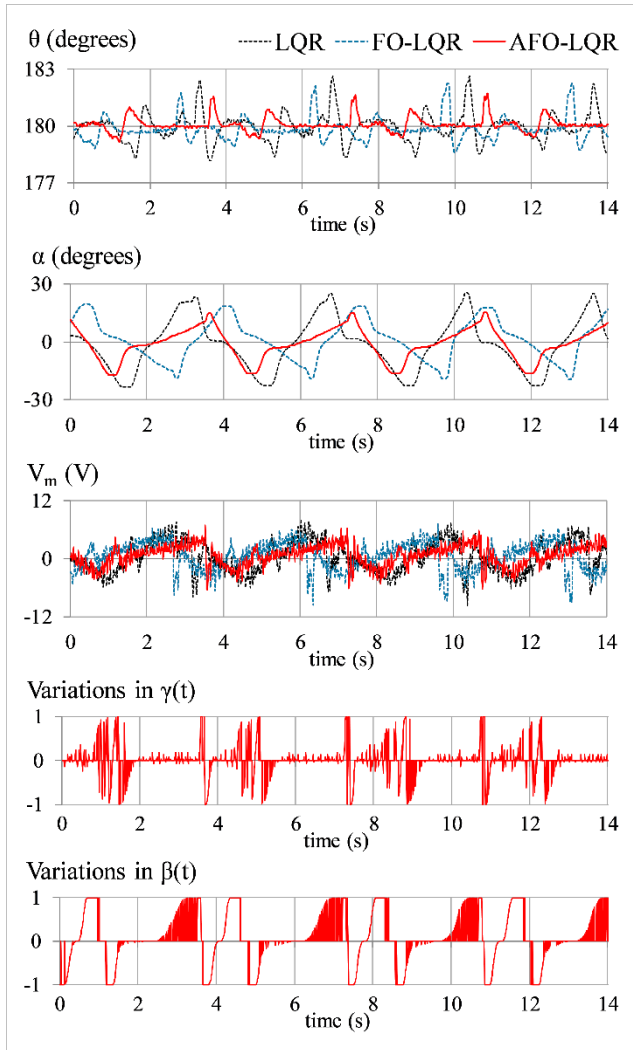


FIGURE 10. System's position regulation under impulsive disruptions.

C. COMPARATIVE PERFORMANCE ASSESSMENT

The results of the aforesaid experiments are comparatively examined via the following seven Key Benchmarking Metrics (KBMs): the root-mean-squared value of state error ($e_{x,RMS}$) in α and θ , the rod's transient recovery span ($t_{set,\theta}$), the magnitude of peak overshoot or undershoot ($|OS_\theta|$) in rod, the step disruption-induced offset (α_{off}) in the arm, the amplitude of the step disruption-induced fluctuations (α_{p-p}) in the arm, the mean squared value of motor voltage (MSV_m), the peak motor voltage (V_p) under transient disturbances [34]. Table III quantifies the experimental results in terms of the aforesaid KBMs. The quantitative data analysis validates the significant improvement contributed by the proposed AFO-LQR in the system's position regulation behavior.

Experiment 1 (Fig. 9) shows that the AFO-LQR outperforms the fixed-gain controllers by minimizing the tracking error while delivering a reasonably better control-input efficiency. The proposed AFO-LQR reduces the system's $e_{\theta,RMS}$ by 32.72%, $e_{\alpha,RMS}$ by 29.23%, and control energy expenditure by 33.56%, in comparison to the baseline LQR.

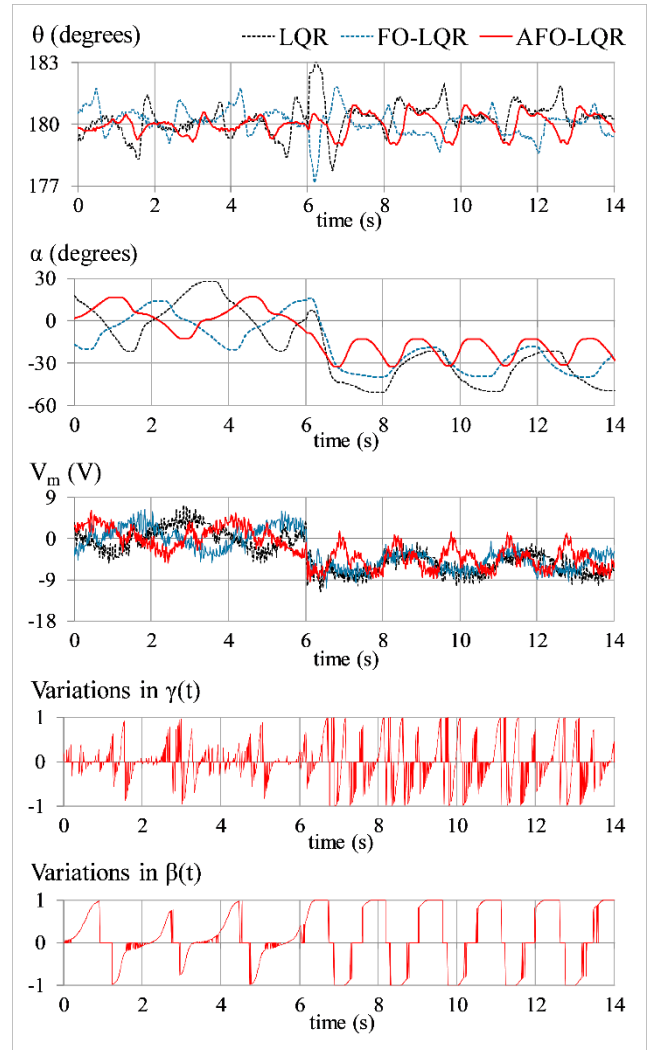


FIGURE 11. System's position regulation under step disruptions.

Experiment 2 (Fig. 10) shows that AFO-LQR delivers a comparatively faster transient recovery speed than the LQR and the FO-LQR while robustly attenuating the overshoots and economizing the control energy requirements. The proposed AFO-LQR reduces the system's transient recovery time by 35.8% and the magnitude of peak overshoots by 35.1%, in comparison to the LQR.

Experiment 3 (Fig. 11) shows that the AFO-LQR surpasses the LQR and FO-LQR by rendering a relatively larger reduction in α_{off} and α_{p-p} without degrading the control energy efficiency. The proposed AFO-LQR reduces the system's α_{off} by 38.2% and α_{p-p} by 34.0%, compared to the LQR.

Experiment 4 (Fig. 12) shows that the AFO-LQR effectively reduces the chattering content, tracking errors to dampen the sinusoidal disturbances without substantially compromising the control input economy. As compared to the LQR, the proposed AFO-LQR dampens the chattering in the pendulum rod's response by 42.6%.

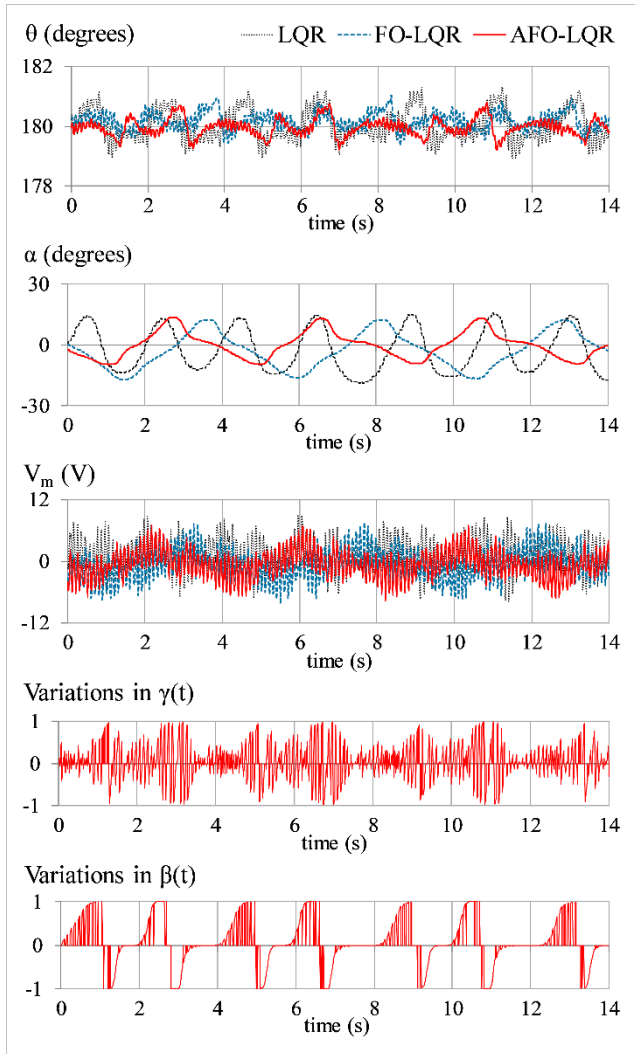


FIGURE 12. System's position regulation under sinusoidal disruptions.

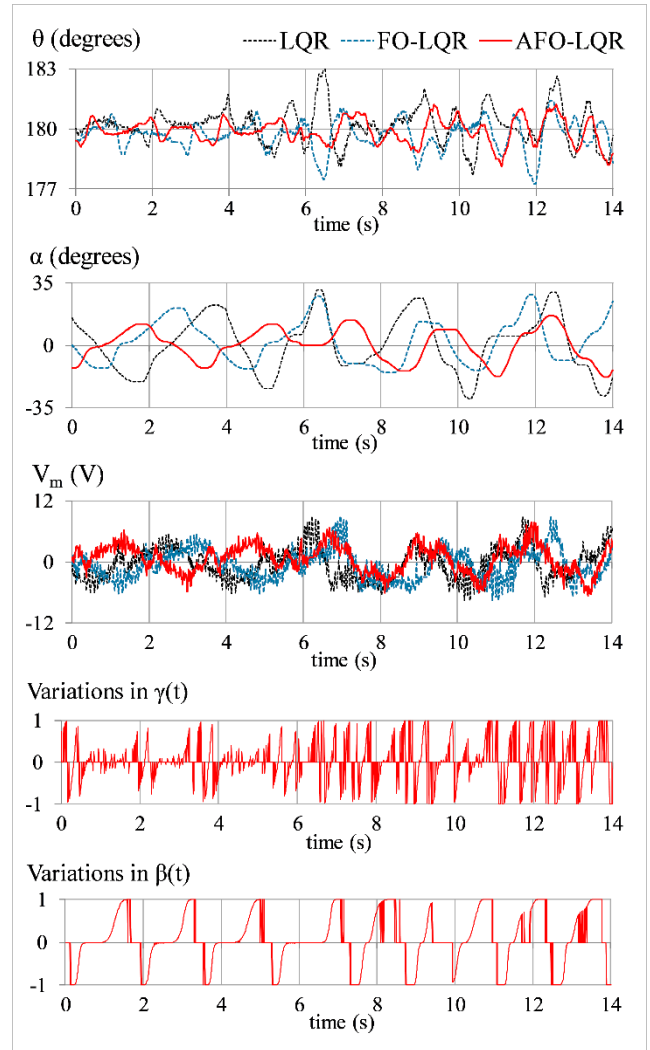


FIGURE 13. System's position regulation under model uncertainties.



FIGURE 13. Pendulum setup with 0.10 kg mass attached to arm [34]

Experiment 5 (Fig. 13) shows that the AFO-LQR yields relatively stronger damping against the perturbations caused by model variations while curbing large servo demands, in comparison to the other two fixed gain controller variants. As compared to the baseline LQR, the proposed AFO-LQR reduces the system's $e_{\theta,RMS}$ by 31.52%, $e_{\alpha,RMS}$ by 39.72%, and control energy expenditure by 36.53%.

The performance of the proposed AFO-LQR is compared with the CFO-LQIR controller proposed in [25] to verify its efficacy against the state-of-the-art controllers. The CFO-LQIR is chosen because its real-time behavior is analyzed on the same RIP experimental setup as used in this research under the same testing scenarios. The comparative performance analysis is quantified in Table IV. The quantitative analysis justifies that the AFO-LQR manifests a significantly improved position regulation behavior and disturbance rejection capability than the CFO-LQIR in almost every testing scenario.

TABLE III
OVERVIEW OF THE EXPERIMENTAL OUTCOMES

Experiment	KBM		Control Procedure		
	Symbol	Units	LQR	FO-LQR	AFO-LQR
1	$e_{\theta,RMS}$	deg.	0.55	0.42	0.35
	$e_{\alpha,RMS}$	deg.	13.34	11.29	9.44
	MSV_m	V^2	7.42	6.57	4.93
2	$e_{\theta,RMS}$	deg.	0.71	0.58	0.38
	$ OS_0 $	deg.	2.62	2.24	1.70
	$t_{set,0}$	sec.	0.81	0.73	0.51
	$e_{\alpha,RMS}$	deg.	13.49	10.34	8.87
	MSV_m	V^2	9.81	8.22	6.16
	V_p	V	-9.73	-9.62	-7.25
3	$e_{\theta,RMS}$	deg.	0.77	0.62	0.52
	$e_{\alpha,RMS}$	deg.	30.97	24.18	18.27
	α_{off}	deg.	-36.68	-29.71	-20.44
	α_{p-p}	deg.	29.05	27.68	19.18
	MSV_m	V^2	25.78	20.35	19.34
	V_p	V	-11.67	-10.93	-8.98
4	$e_{\theta,RMS}$	deg.	0.54	0.37	0.30
	$e_{\alpha,RMS}$	deg.	10.98	9.33	6.61
	MSV_m	V^2	10.91	9.39	7.33
5	$e_{\theta,RMS}$	deg.	0.92	0.84	0.63
	$e_{\alpha,RMS}$	deg.	15.46	12.93	9.32
	MSV_m	V^2	12.73	9.97	8.08

The outcomes of these experiments validate the improved adaptability and resilience to the exogenous disturbances provided by the AFO-LQR. The AFO-LQR's flexible control yield is credited to the rule-based abrupt changes in the controller's FOs in response to state error-phase variations, which systematically mutates the nominal FO-LQR structure from a predominantly PD-type to PI-type controller.

TABLE IV
EXPERIMENTAL COMPARISON WITH CFO-LQIR [25]

Experiment	KBM		Control Procedure		Percentage Improvement
	Symbol	Units	CFO-LQIR [25]	AFO-LQR	
1	$e_{\theta,RMS}$	deg.	0.36	0.35	2.8 %
	$e_{\alpha,RMS}$	deg.	10.08	9.44	6.3 %
	MSV_m	V^2	7.18	4.93	31.3 %
2	$e_{\theta,RMS}$	deg.	0.47	0.38	19.1 %
	$ OS_0 $	deg.	2.23	1.70	23.8 %
	$t_{set,0}$	sec.	0.51	0.51	0.0 %
	$e_{\alpha,RMS}$	deg.	9.68	8.87	8.4 %
	MSV_m	V^2	6.39	6.16	3.6 %
	V_p	V	-8.47	-7.25	14.4 %
3	$e_{\theta,RMS}$	deg.	0.42	0.52	-23.8 %
	$e_{\alpha,RMS}$	deg.	22.06	18.27	17.2 %
	α_{off}	deg.	-23.72	-20.44	13.8 %
	α_{p-p}	deg.	21.61	19.18	11.2 %
	MSV_m	V^2	25.35	19.34	23.7 %
	V_p	V	-10.34	-8.98	13.2 %
4	$e_{\theta,RMS}$	deg.	0.29	0.30	-3.4 %
	$e_{\alpha,RMS}$	deg.	9.53	6.61	30.6 %
	MSV_m	V^2	10.50	7.33	30.2 %
5	$e_{\theta,RMS}$	deg.	0.78	0.63	19.2 %
	$e_{\alpha,RMS}$	deg.	11.78	9.32	20.9 %
	MSV_m	V^2	9.48	8.08	14.8 %

Adaptive FOs are more responsive to the system's error conditions or external disturbances, allowing the system to maintain robust-optimal performance under varying conditions. By adapting the FO as needed, the closed-loop system operates more efficiently, effectively reducing the overshoots, improving the response time, economizing the control energy application, and reducing wear and tear on the actuator. This behavior is evident in the experimental results as well. The aforementioned traits enable the AFO-LQR to robustly compensate for bounded external disturbances and model variations.

The proposed control procedure can contribute immensely to the field of under-actuated robotics and mechatronics. The AFO-LQR's structure provides more degrees of freedom, which enhances the system's robustness against disturbances that are commonly encountered in robotic applications, such as variations in payload, changing environmental conditions, or mechanical wear and tear. Furthermore, robotic applications often involve systems with complex dynamics that may exhibit non-integer order behavior. The proposed controller is better equipped to capture such a system's dynamics accurately, leading to improved performance and stability. The adaptability of the proposed control law enables it to flexibly manipulate the stiffness of the applied control input as per the variations in the system's state error phase. Apart from the robotic applications, the AFO-LQR can be used in aircraft flight control systems to provide superior handling of turbulent conditions and unexpected disturbances. It can be used in satellite attitude control systems to manage the orientation of satellites more effectively, accounting for the complex dynamics and external perturbations in space. This scheme can also be beneficial in robustly handling the vehicles by dynamically adjusting their suspension and steering systems. Finally, it can optimize the performance of renewable energy converters by quickly adapting to changing environmental conditions.

V. CONCLUSION

This article proposes a novel self-tuning AFO-LQR scheme driven by a phase-based adaptation law to improve the adaptability of inverted-pendulum-type robots. To achieve the desired control objectives, the nominal LQR for RIP systems is augmented with fractional calculus. Fractional calculus is widely used to model and control complex dynamical systems that cannot be accurately described by traditional integer-order calculus. The experimental results affirm that the AFO-LQR provides better position regulation, disturbance attenuation, and cost-effective control activity. The proposed control structure provides more degrees of freedom, which enhances the system's robustness against disturbances commonly encountered in robotic applications, such as variations in payload, changing environmental conditions, or mechanical wear and tear. Furthermore, robotic applications often involve systems with complex dynamics that may exhibit non-integer order behavior. The proposed controller is better equipped to

capture such a system's dynamics accurately, leading to improved performance and stability. The AFO-LQR is scalable and can work with various systems, provided that the new system's nominal state space model and its tailored FO adaptation functions are attainable beforehand.

There is indeed a lot of room for future enhancements. In the future, the proposed AFO-LQR scheme can be extended and applied to energy conversion or flight control systems to ascertain its efficacy with other potential applications. state-of-the-art soft computing techniques can be used to adaptively modulate the FOs and evaluate the consequent implications. Relative rate feedback can be augmented with the traditional FO-LQR to investigate its impact on the execution of online self-tuning of FOs.

REFERENCES

- [1] O. Saleem and J. Iqbal, "Fuzzy-Immune-Regulated Adaptive Degree-of-Stability LQR for a Self-Balancing Robotic Mechanism: Design and HIL Realization," *IEEE Robot. Autom. Lett.*, vol. 8, no. 8, pp. 4577-4584, Aug. 2023.
- [2] M. Ramírez-Neria, H. Sira-Ramírez, R. Garrido-Moctezuma and A. Luviano-Juarez, "Linear active disturbance rejection control of underactuated systems: The case of the Furuta pendulum," *ISA Trans.*, vol. 53, no. 4, pp. 920-928, 2014.
- [3] M. Waszak and R. Łangowski, "An Automatic Self-Tuning Control System Design for an Inverted Pendulum," *IEEE Access*, vol. 8, pp. 26726-26738, Feb. 2020.
- [4] F. F. M. El-Sousy, K. A. Alattas, O. Mofid, S. Mobayen and A. Fekih, "Robust Adaptive Super-Twisting Sliding Mode Stability Control of Underactuated Rotational Inverted Pendulum With Experimental Validation," *IEEE Access*, vol. 10, pp. 100857-100866, Sep. 2022.
- [5] N. P. Nguyen, H. Oh, Y. Kim, J. Moon, J. Yang and W. -H. Chen, "Fuzzy-Based Super-Twisting Sliding Mode Stabilization Control for Under-Actuated Rotary Inverted Pendulum Systems," *IEEE Access*, vol. 8, pp. 185079-185092, Oct. 2020.
- [6] A. Nagarajan and A. A. Victoire, "Optimization Reinforced PID-Sliding Mode Controller for Rotary Inverted Pendulum," *IEEE Access*, vol. 11, pp. 24420-24430, Mar. 2023.
- [7] O. Saleem, J. Iqbal and M. Rizwan, "Adaptive Optimal Control of Under-actuated Robotic Systems using a Self-Regulating Nonlinear Weight-Adjustment Scheme: Formulation and Experimental Verification," *Plos one*, vol. 18, no. 12, e0295153, Dec. 2023.
- [8] Z. Li, C. Yang and L. Fan, L., *Advanced Control of Wheeled Inverted Pendulum Systems*. London, UK: Springer, 2013.
- [9] J. J. Wang, "Simulation studies of inverted pendulum based on PID controllers," *Simul. Model. Pract. Theory*, vol. 19, no. 1, pp. 440-449, Jan. 2011.
- [10] N. P. Nguyen, H. Oh, Y. Kim, J. Moon, J. Yang and W. -H. Chen, "Fuzzy-Based Super-Twisting Sliding Mode Stabilization Control for Under-Actuated Rotary Inverted Pendulum Systems," *IEEE Access*, vol. 8, pp. 185079-185092, Oct. 2020.
- [11] S. Ullah, Q. Khan, M. M. Zaidi and L. G. Hua, "Neuro-adaptive non-singular terminal sliding mode control for distributed fixed-time synchronization of higher-order uncertain multi-agent nonlinear systems," *Inf. Sci.*, vol. 659, 120087, Feb. 2024.
- [12] S. Ullah, A. Mehmood, Q. Khan, S. Rehman and J. Iqbal, "Robust Integral Sliding Mode Control Design for Stability Enhancement of Under-actuated Quadcopter," *Int. J. Control Autom. Syst.*, vol. 18, pp. 1671-1678, Feb. 2020.
- [13] K. Ali, S. Ullah, A. Mehmood, H. Mostafa, M. Marey and J. Iqbal, "Adaptive FIT-SMC Approach for an Anthropomorphic Manipulator With Robust Exact Differentiator and Neural Network-Based Friction Compensation," *IEEE Access*, vol. 10, pp. 3378-3389, Jan. 2022.
- [14] M. Munir, Q. Khan, S. Ullah, T. M. Syeda, A. A. Alghamhi, "Control Design for Uncertain Higher-Order Networked Nonlinear Systems via an Arbitrary Order Finite-Time Sliding Mode Control Law," *Sensors*, vol. 22, no. 7, 2748, Apr. 2022.
- [15] X. Wang, B. Wang, X. Chen and J. Yu, "Discrete-Time Position Tracking Control for Multimotor Driving Systems via Multipower Terminal Sliding-Mode Technique," *IEEE/ASME Trans. Mechatron.*, vol. 29, no. 2, pp. 1158-1169, Apr. 2024.
- [16] X. Wang, B. Wang, X. Chen and J. Yu, "Characteristic Model-Based Discrete-Time Adaptive Tracking Control for Multimotor Driving Systems With Inertia Variations," *IEEE Trans. Transp. Electr.*, doi: 10.1109/TTE.2024.3396653.
- [17] M. Huba and D. Vrancic, "Extending the model-based controller design to higher-order plant models and measurement noise," *Symmetry*, vol. 13, no. 5, 798, 2021.
- [18] O. Saleem, "An enhanced adaptive-LQR procedure for under-actuated systems using relative-rate feedback to dynamically reconfigure the state-weighting-factors," *J. Vib. Control*, vol. 29, no. 9-10, pp. 2316-2331, May 2023.
- [19] H. -Y. Zhang, J. Wang and G. -D. Lu, "Self-organizing fuzzy optimal control for under-actuated systems," *J. Syst. Control Eng.*, vol. 228, no. 8, pp. 578-590, 2021.
- [20] O. Saleem, K. Mahmood-ul-Hasan and M. Rizwan, "An experimental comparison of different hierarchical self-tuning regulatory control procedures for under-actuated mechatronic systems," *Plos One*, vol. 16, no. 8, e0256750, 2021.
- [21] F. Waheed, I. Khan Yousufzai and M. Valášek, "A TV-MPC Methodology for Uncertain Under-Actuated Systems: A Rotary Inverted Pendulum Case Study," *IEEE Access*, vol. 11, pp. 103636-103649, Sep. 2023.
- [22] C. Yang, Z. Li and J. Li J, "Trajectory planning and optimized adaptive control for a class of wheeled inverted pendulum vehicle models," *IEEE Trans. Cybern.*, vol. 43, no. 1, pp. 24-36, Jun. 2012.
- [23] P. Dwivedi, S. Pandey and A.S. Junghare, "Robust and novel two degree of freedom fractional controller based on two-loop topology for inverted pendulum," *ISA Trans.*, vol. 75, pp. 189-206, Apr. 2018.
- [24] O. Saleem, K. Mahmood-ul-Hasan, "Robust stabilisation of rotary inverted pendulum using intelligently optimised nonlinear self-adaptive dual fractional-order PD controllers," *Int J. Syst. Sci.*, vol. 50, no. 7, pp. 1399-1414, May 2019.
- [25] O. Saleem, F. Abbas and J. Iqbal, "Complex Fractional-Order LQIR for Inverted-Pendulum-Type Robotic Mechanisms: Design and Experimental Validation," *Mathematics*, vol. 11, no. 4, 913, 2023.
- [26] O. W. Abdulwahhab, "Design of a complex fractional order PID controller for a first order plus time delay system," *ISA Trans*, vol. 99, pp. 154-158, 2020.
- [27] M. Shahiri, A. Ranjbar, M. Karami, R. Ghaderi, "Robust control of nonlinear PEMFC against uncertainty using fractional complex order control," *Nonlinear Dyn.*, vol. 80, pp. 1785-1800, 2015.
- [28] S. Balamurugan and P. Venkatesh, "Fuzzy sliding-mode control with low pass filter to reduce chattering effect: an experimental validation on Quanser SRIP," *Sadhana*, vol. 42, no. 10, pp. 1693-1703, Oct. 2017.
- [29] K. J. Astom, J. Apkarian, P. Karam, M. Levis, J. Falcon, *Student Workbook: QNET Rotary Inverted Pendulum Trainer for NI ELVIS*. Ontario, Canada: Quanser, 2011.
- [30] D. Xue, Y. Q. Chen and D. P. Atherton, *Linear Feedback Control: Analysis and Design with MATLAB*. Philadelphia, USA: SIAM, 2007.
- [31] O. Saleem, M. Rizwan, "Performance optimization of LQR-based PID controller for DC-DC buck converter via iterative-learning-tuning of state-weighting matrix," *Int. J. Numer. Model.*, vol. 32, no. 3, e2572, May/June 2019.
- [32] Z. Li, L. Liu, S. Dehghan, Y. Q. Chen and D. Xue, "A review and evaluation of numerical tools for fractional calculus and fractional order controls," *Int. J. Control*, vol. 90, no. 6, pp. 1165-1181, Jan. 2017.

- [33] O. W. Abdulwahhab and N. H. Abbas, "A New Method to Tune a Fractional-Order PID Controller for a Twin Rotor Aerodynamic System," *Arab. J. Sci. Eng.*, vol. 42, pp. 5179–5189, 2017.
- [34] O. Saleem, K. Mahmood-UI-Hasan, "Indirect Adaptive State-Feedback Control of Rotary Inverted Pendulum Using Self-Mutating Hyperbolic-Functions for Online Cost Variation," *IEEE Access*, vol. 8, pp. 91236-91247, May 2020.
- [35] B. S. Armstrong, J. A. Gutierrez, B. A. Wade and R. Joseph, "Stability of phase-based gain modulation with designer-chosen switch functions," *Int. J. Robot. Res.*, vol. 25, no. 8, pp. 781-796, Aug. 2006.
- [36] O. Saleem, K. Mahmood-ul-Hasan, "Hierarchical Adaptive Control of Self-Stabilizing Electromechanical Systems using Artificial-Immune Self-Tuning Mechanism for State Weighting-Factor," *J. Mech. Sci. Technol.*, vol. 35, pp. 1235–1250, Mar. 2021.
- [37] B. B. Alagoz, A. Ates, C. Yeroglu and B. Senol "An experimental investigation for error-cube PID control," *Trans. Inst. Meas Control*, vol. 37, no. 5, pp. 652-660, May 2015.
- [38] "Pulse Pattern," (2024, Jan. 31). Accessed on: Mar. 23, 2024. [Online]. Available: <https://www.ni.com/docs/en-US/bundle/labview-api-ref/page/vi-lib/analysis/1siggen-llb/pulse-pattern-vi.html>



Omer Saleem (Senior Member, IEEE) received his Ph.D. degree in adaptive control systems from University of Engineering and Technology, Lahore, Pakistan, in 2021. He is currently working as an Associate Professor of Electrical Engineering at FAST - National University of Computer and Emerging Sciences, Lahore, Pakistan. His research interests include adaptive optimal and self-tuning control of self-balancing robots. He is on the editorial board of several reputed journals.



Jamshed Iqbal (Senior Member, IEEE) received three M.S. degrees in various fields of engineering from Finland, Sweden, and Pakistan, respectively, and Ph.D. degree in robotics from the Italian Institute of Technology (IIT). He is currently working as a Senior Lecturer in University of Hull, U.K. He has more than 20 years of multi-disciplinary experience in industry and academia. He is on the editorial board of several reputed journals and program committee member of various IEEE international conferences.